# SUPPLEMENTARY INFORMATION

doi:10.1038/nature09369

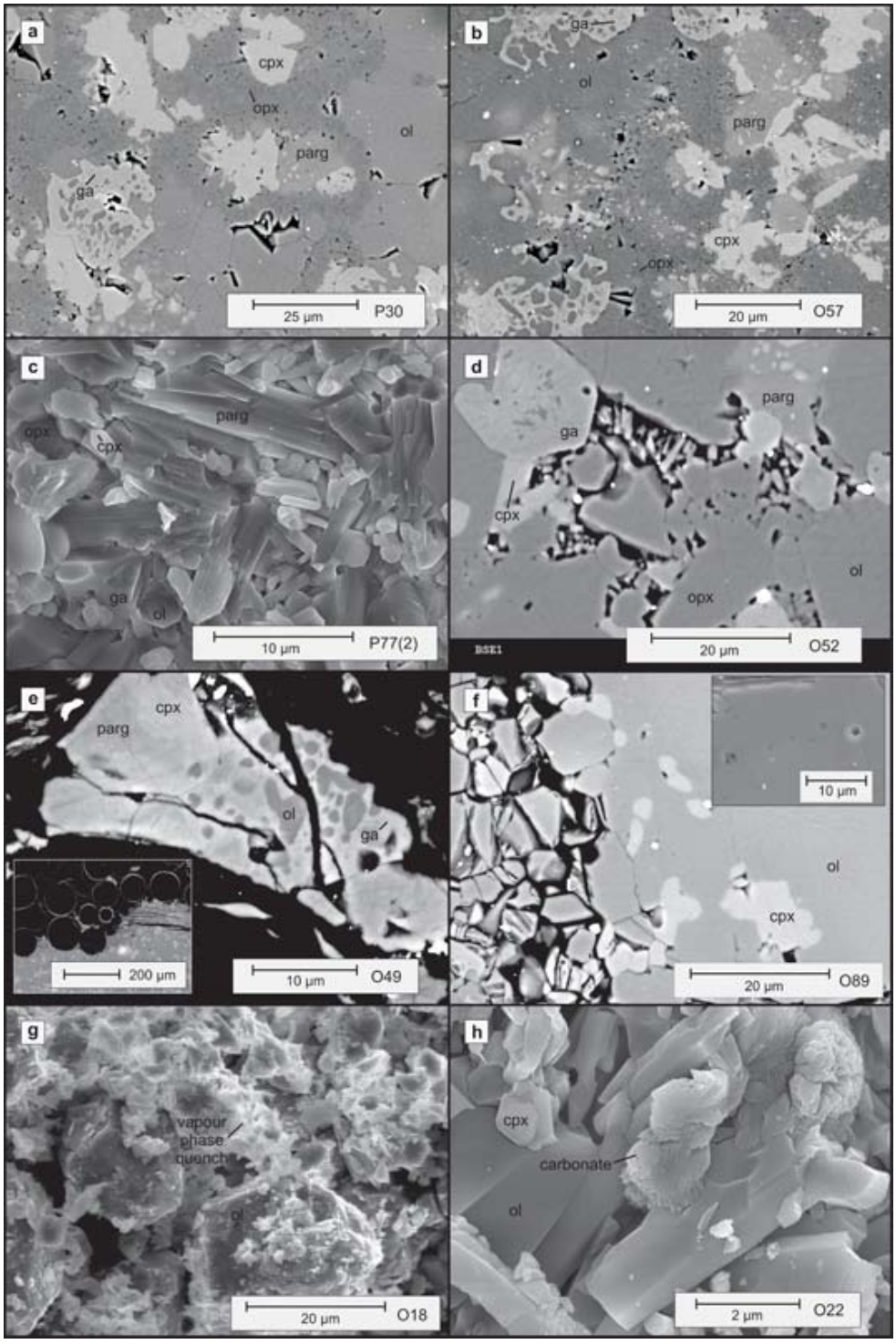


**Supplementary Figure S1 | Scanning electron microscope images of experimental charges with vapour and vapour phase quench.** Experimental runs are in the order of added water concentration from the lowest wt.% of added $H_2O$ to highest wt.% of added $H_2O$. parg – pargasite, ga – garnet, cpx – clinopyroxene, opx – orthopyroxene, ol – olivine.

A) Experiment D968 (P30) HZ1 lherzolite composition at 2.5 GPa, 1000°C, dry (i.e. no $H_2O$ added). Back-scattered electron image of polished surfaces of pargasite lherzolite. The order of decreasing 'brightness' in the images is clinopyroxene > garnet (poikilitic) > pargasite > olivine > orthopyroxene, similar as in B) and C). Pargasite grains are right of the centre. Although nominally 'dry', the presence of pargasite indicates that trace water/hydrogen gained access. Also note the lower intergranular void space in A) and B) relative to D) (1.45 wt.% $H_2O$).

B) Experiment C2901 (O57) HZ2 lherzolite composition at 2.5 GPa, 1000°C, 0.073 wt.% $H_2O$. Back-scattered electron image of polished surfaces of pargasite lherzolite. Pargasite grains are in the upper right of the image.

C) Experiment D1036 (P77(2)) HZ1 lherzolite composition at 1.5 GPa, 950°C, ~1 wt.% $H_2O$. Secondary electron image of lherzolite with excess water-rich vapour showing pargasite intergrowth with olivine and pyroxenes. Broken surface illustrating crystal faces against voids (vapour). Pargasite in the upper centre.

D) Experiment C2886 (O52) HZ2 composition at 2.5 GPa, 1025°C, 1.45 wt.% $H_2O$. Back-scattered electron image of polished surfaces of pargasite lherzolite. Pargasite grains are in the upper right of the image. Pargasite increases in abundance A, B, D as shown by decreasing $K_2O$ in pargasite.

E) Experiment C2876 (O49) HZ2 lherzolite composition at 2.5 GPa, 1025°C, 1.45 wt.% $H_2O$. Back-scattered electron image of edge of pargasite-bearing garnet lherzolite layer against the layer of carbon spheres. Silicate minerals between spheres are not quenched from silicate melt or vapour phase but are pargasite (the most common phase), clinopyroxene, orthopyroxene, garnet and olivine with compositions identical with those of the lherzolite layer, except for vanishingly small $Cr_2O_3$ contents in all phases. The minerals are interpreted as void-filling growth of equilibrium phases by element transport through the vapour phase.

F) Experiment C2919 (O89) HZ2 lherzolite composition at 2.5 GPa, 1000°C, 7.25 wt.% $H_2O$. Back-scattered electron image of fragment of olivine disc within garnet lherzolite. The olivine single crystal shows an open fracture along which olivine is replaced by clinopyroxene giving a discontinuous clinopyroxene veinlet. Olivine close to the fracture or disc edge is ~$Mg_{93.5}$ whereas olivine at >10 microns from the fracture has $Mg_{91}$. The insert is a secondary electron image of a train of fluid inclusions within the same olivine disc.

G) Experiment C2836 (O18) HZ2 lherzolite composition at 2.4 GPa, 960°C, 14.5 wt.% $H_2O$. Euhedral olivine crystals with fragmented thin films of silica-rich glass (secondary electron image).

H) Experiment C2841 (O22) HZ2 lherzolite composition at 2.8 GPa, 840°C, 14.5 wt.% $H_2O$. Quench 'rosette' of carbonate and glass fragments adhering to euhedral pyroxene and olivine crystals (secondary electron image).

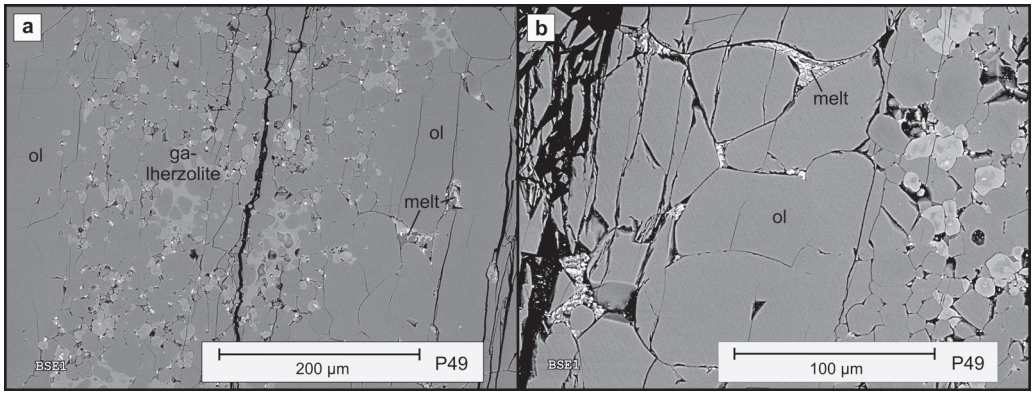


**Supplementary Figure S2 | Scanning electron microscope images of experimental charges with quench from water-rich silicate melt of experiment UHPPC114 (P49) HZ1 lherzolite composition at 6 GPa, 1400°C, 1.45 wt.% $H_2O$.** Abbreviations as in Supplementary Figure S1.

A) Back-scattered electron image of lherzolite layer between two olivine layers. Recrystallization and grain growth of olivine is accompanied by migration of hydrous silicate melt into the 'olivine melt trap'.

B) Back-scattered electron image of olivine layer with lherzolite layer. Image shows interserts of quench clinopyroxene, oxide and carbonate, and quench rims on olivine.

**Supplementary Table S3 | Experimental conditions and results on 'HZ1' composition.** HZ1 and MOR Pyrolite are estimates of the upper mantle composition in the region acting as the source for MORB i.e. the asthenosphere.

| Run No. | Mount No. | T (°C) | Time (days) | wt.% $H_2O$ | Capsule | Top L | Bottom L | Phase assemblage (with OL+OPX+CPX) SP/GA | PAR | Melt | Vap |
|---|---|---|---|---|---|---|---|---|---|---|---|
| *HZ1 Peridotite at 1.5 GPa* | | | | | | | | | | | |
| D1036 | P77(2) | 950 | 4 | ~1 | Au | - | - | SP | PAR | - | Vap |
| D1041 | P82 | 1025 | 3 | ~0.05 | Au | OL(SC) | OL(SC) | SP | PAR | - | - |
| C3230 | P83 | 1025 | 3 | ~0.3 | Au | OL(SC) | OL(SC) | SP | PAR | - | - |
| *HZ1 Peridotite at 2.5 GPa* | | | | | | | | | | | |
| D968 | P-30 | 1000 | 7 | DRY | Au | OL(SC) | Lo-Al Opx | GA | PAR | - | - |
| D1039 | P80 | 1000 | 3 | ~0.3 | Au | OL(SC) | OL(SC) | GA | PAR | - | - |
| D897 | O-85 | 1000 | 2.7 | 1.45 | Ag | OL(SC) | OL(SC) | GA | PAR | - | Vap |
| D937 | P-4 | 1000 | 7 | 1.45 | Au | Hi-Al Opx | Hi-Al Cpx | GA | - | - | Vap |
| D944 | P-7 | 1000 | 7 | 1.45 | Au | Lo-Al Opx | Lo-Al Cpx | GA | - | - | Vap |
| C3225 | P81 | 1025 | 3 | ~0.3 | Au | OL(SC) | OL(SC) | GA | PAR | Melt[a] | |
| C2936 | O-79 | 1025 | 3 | 1.45 | Ag | OL(SC) | OL(SC) | GA | - | Melt[a] | Vap |
| D1038 | P78 | 1050 | 3 | ~0.05 | Au | OL(SC) | OL(SC) | GA | PAR | - | - |
| C3222 | P79 | 1050 | 3 | ~0.3 | Au | OL(SC) | OL(SC) | GA | - | Melt[a] | - |
| C2930 | O-77 | 1050 | 3 | 1.45 | Ag | OL(SC) | OL(SC) | GA | - | Melt[a] | - |
| *HZ1 Peridotite at 3.0 GPa* | | | | | | | | | | | |
| D1035 | P77(1) | 950 | 4 | ~0.5 | Au | - | - | GA | PAR | - | Vap |
| *HZ1 Peridotite at 4.0 GPa* | | | | | | | | | | | |
| C2987 | O-92 | 1100 | 4 | 0.145 | Au | OL(SC) | OL(SC) | GA | - | - | Vap |
| C2942 | O-80 | 1100 | 3 | 1.45 | Au | OL(SC) | OL(SC) | GA | - | - | Vap |
| C2935 | O-78 | 1150 | 3 | 1.45 | Au | OL(SC) | OL(SC) | GA | - | - | Vap |

| | | | | | | | | | | | |
|---|---|---|---|---|---|---|---|---|---|---|---|
| C3005 | P-3 | 1150 | 7 | 1.45 | Au | Hi-Al Opx | Hi-Al Cpx | GA | - | - | Va |
| C3010 | P-6 | 1150 | 7 | 1.45 | Au | Lo-Al Opx | Lo-Al Cpx | GA | - | - | Va |
| C2950 | O-81 | 1200 | 3 | 1.45 | Au | OL(SC) | OL(SC) | GA | - | - | Va |
| C2899 | O-98/99 | 1225 | 1 | 1.45 | AuPd | OL(SC) | OL(SC) | GA | - | Melt[a] | - |
| | | | | | | | | | | | |
| *HZ1 Peridotite at 6.0 GPa* | | | | | | | | | | | |
| UHPPC117 | P53 | 1300 | 12h | 1.45 | AuPd | OL(SC) | OL(SC) | GA | - | - | ?Va |
| UHPPC116 | P51 | 1350 | 12h | 0.145 | AuPd | OL(SC) | OL(SC) | GA | - | - | ?Va |
| UHPPC129 | P84 | 1350 | 12h | ~1 | AuPd | 1/3 OL | | GA | - | - | ?Va |
| UHPPC95 | P-21 | 1350 | 3 | 1.45 | AuPd | OL(SC) | Lo-Al Opx | GA | - | - | ?Va |
| UHPPC131 | P86 | 1400 | 12h | ~1 | AuPd | 1/3 OL | | GA | - | Melt[a] | - |
| UHPPC113 | P47 | 1400 | 12h | 1.45 | AuPd | OL(SC) | Lo-Al Opx | GA | - | Melt[a] | - |
| UHPPC114 | P49 | 1400 | 12h | 1.45 | AuPd | OL(SC) | OL(SC) | GA | - | Melt[a] | - |
| UHPPC130 | P85 | 1450 | 4.5h | ~1 | AuPd | 1/3 OL | | GA | - | Melt[a] | - |

OL, olivine; OPX, orthopyroxene; CPX, clinopyroxene; SP, Spinel; GA, garnet; PAR, pargasite; Vap, vapour; L, Layer; C-Sph, Carbon-spheres; Lo-Al OPX, Low alumina orthopyroxene; Hi-Al OPX, High alumina orthopyroxene; OL(SC), San Carlos olivine; AuPd, AuPd double capsule; [a], Quench materials of cpx or amp, oxide and carbonate - hydrous silicate melt quench; [b], Quench materials of dolomite, minor oxide and minor Na-Si-rich silicate – Fluid phase or carbonatitic melt quench.

**Supplementary Table S4 | Experimental conditions and results on 'HZ2' composition.**

| Run# | Mount# | T (°C) | Time (days) | wt.% $H_2O$ | Capsule | Top L | Bottom L | Phase assemblage (with OL+OPX+CPX+GA) | | |
|---|---|---|---|---|---|---|---|---|---|---|
| | | | | | | | | PAR | Melt | Vap |
| *HZ2 Peridotite at 2.0 GPa* | | | | | | | | | | |
| C2866 | O-35,38 | 850 | 3 | 14.5 | Ag | C-Sph | C-Sph | PAR | - | Vap |
| C2848 | O-26 | 940 | 7 | 1.45 | Au | - | - | PAR | - | Vap |
| *HZ2 Peridotite at 2.4 GPa* | | | | | | | | | | |
| C2842 | O-24 | 960 | 6 | 1.45 | Au | - | - | PAR | - | Vap |
| C2836 | O-17,18 | 960 | 4 | 14.5 | Au | - | - | - | - | Vap |
| C2835 | O-16[a] | 1100 | 3 | DRY | Au | - | - | - | - | - |
| *HZ2 Peridotite at 2.5 GPa* | | | | | | | | | | |
| C2911 | O-65 | 1000 | 7 | DRY | G-Ag[b] | - | - | PAR | - | - |
| C2901 | O-57 | 1000 | 1 | 0.073 | Ag | - | - | PAR | - | - |
| C2900 | O-56 | 1000 | 1 | 0.145 | Ag | - | - | PAR | - | ?Vap |
| D879 | O-70 | 1000 | 1 | 0.725 | Ag | C-Sph | C-Sph | PAR | - | Vap |
| C2867 | O-36 | 1000 | 3 | 1.45 | Ag | C-Sph | C-Sph | PAR | - | Vap |
| C2888 | O-60 | 1000 | 3 | 2.9 | Ag | | OL-Disc | PAR | - | Vap |
| C2919 | O-89 | 1000 | 1 | 7.25 | Ag | | OL-Disc | - | - | Vap |
| C2877 | O-50 | 1000 | 3 | 14.5 | Ag | C-Sph | C-Sph | - | - | Vap |
| C2876 | O-49 | 1025 | 3 | 1.45 | Ag | C-Sph | C-Sph | PAR | - | Vap |
| C2886 | O-52 | 1025 | 3 | 1.45 | Ag | OL(SC) | OL(SC) | PAR | - | Vap |
| C2909 | O-62 | 1050 | 3 | 1.45 | Ag | C-Sph | C-Sph | PAR | - | Vap |
| C2887 | O-53 | 1050 | 3 | 1.45 | Ag | OL(SC) | OL(SC) | - | Melt | - |
| D881 | O-72 | 1075 | 1 | 1.45 | Ag | C-Sph | C-Sph | PAR | - | Vap |
| *HZ2 Peridotite at 2.8 GPa* | | | | | | | | | | |
| C2841 | O-22,23 | 840 | 7 | 14.5 | Au | - | - | - | - | Vap |

| | | | | | | | | | | |
|---|---|---|---|---|---|---|---|---|---|---|
| C2849 | O-27 | 950 | 7 | 1.45 | Au | - | - | PAR | - | Vap |
| *HZ2 Peridotite at 3.0 GPa* | | | | | | | | | | |
| D880 | O-71 | 1000 | 3 | 0.145 | Ag | - | - | PAR | - | ?Vap |
| C2924 | O-73 | 1000 | 3 | 1.45 | Ag | C-Sph | C-Sph | PAR | - | Vap |
| *HZ2 Peridotite at 4.0 GPa* | | | | | | | | | | |
| C2889 | O-61 | 1100 | 3 | 2.9 | Ag | OL | Disc | - | - | Vap |
| C2928 | O-76 | 1150 | 1 | 1.45 | Ag | OL(SC) | OL(SC) | - | - | Vap |

[a], Run 2836 (O16) contains Spinel rather than Garnet; [b], Graphite in Ag; OL, olivine; OPX, orthopyroxene; CPX, clinopyroxene; GA, garnet; PAR, pargasite; Vap, Vapour; L, Layer; C-Sph, Carbon-spheres; OL(SC), San Carlos olivine.